Nonmagnetic Impurity Resonances as a Signature of Sign-Reversal Pairing in FeAs-Based Superconductors

Degang Zhang

Texas Center for Superconductivity and Department of Physics, University of Houston, Houston, Texas 77204, USA

(Received 25 April 2009; published 26 October 2009)

The energy band structure of FeAs-based superconductors is fitted by a tight-binding model with two Fe ions per unit cell and two degenerate orbitals per Fe ion. Based on this, superconductivity with extended s-wave pairing symmetry of the form $\cos k_x + \cos k_y$ is examined. The local density of states near an impurity is also investigated by using the T-matrix approach. For the nonmagnetic scattering potential, we found that there exist two major resonances inside the gap. The height of the resonance peaks depends on the strength of the impurity potential. These in-gap resonances are originated in the Andreev's bound states due to the quasiparticle scattering between the hole Fermi surfaces around Γ point with positive order parameter and the electron Fermi surfaces around M point with negative order parameter.

DOI: 10.1103/PhysRevLett.103.186402 PACS numbers: 71.10.Fd, 71.18.+y, 71.20.−b, 74.20.−z

The recent discovery of a new family of superconductors, i.e., the FeAs-based superconductors [1–6], has attracted much attention in the condensed matter community. It has been reported that the superconducting transition temperature T_c can be obtained as high as 55 K [2]. Undoped iron arsenides have a spin density wave order below 150 K [4]. When holes or electrons are doped, the iron arsenides become superconducting.

Similar to cuprate superconductors, FeAs-based superconductors also have a layer structure. It has been accepted that superconductivity comes from Cooper pairs in the Fe-Fe plane. However, in FeAs-based superconductors, each unit cell contains two Fe ions and two As ions. The four As ions around each Fe ion do not locate in the Fe-Fe plane and have a twofold rotation symmetry and two reflection symmetries (see Fig. 1). Because of different arrays of As ions around Fe ions, the Fe-Fe plane can be divided into two sublattices A and B. We note that the diagonal directions of the Fe-Fe plane have translational symmetry with the period a. In this coordinate system, the momentum is a good quantum number.

Angle resolved photoemission spectroscopy (ARPES) experiments have probed electronic properties in FeAs-based superconductors [7–15]. It is established that there are two hole Fermi surfaces around (0,0) and two electron Fermi surfaces around (π, π). These Fermi surface characteristics have been obtained by local-density approximation calculations [16–19]. Many theoretical models have been presented to reproduce the hole and electron pockets by employing Fe d and As p orbitals and the hybridization among them [20–25]. However, there is no consensus on the superconducting gaps on Fermi surfaces. In a series of ARPES, scanning tunneling microscopy (STM) experiments, and point-contact Andreev reflection spectroscopy experiments, the order parameter has been interpreted to be nodeless [7,9–15,26], nodal [27,28], single gap [10,26,29–31], and multiple gaps [7,11–15].

In this Letter, we start from two Fe ions per unit cell and two degenerate orbitals d_{xz} and d_{yz} per Fe ion and construct an effective four-band model, which exhibits the features of Fermi surfaces in FeAs-based superconductors. Based on the mean field theory for superconductivity, we investigate the differential conductance and the impurity effect for the extended s-wave pairing symmetry [12,17,20], so that we can understand the electronic properties in FeAs-based superconductors.

We assume that t_1 is the hopping between the same orbitals on the nearest neighboring Fe sites, t_2 and t_3 are

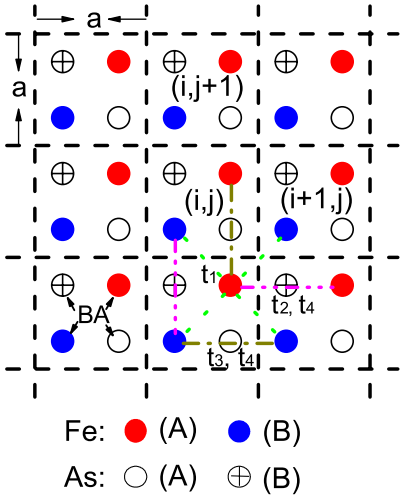

FIG. 1 (color online). Schematic lattice structure of FeAs layers with each unit cell (denoted by i and j) containing two Fe (A and B) and two As (A and B) ions. The As ions A and B are located just above and below the center of each face of the Fe square lattice, respectively. Here, t_1 is the nearest neighboring hopping between the same orbitals d_{xz} or d_{yz}. t_2 and t_3 are the next nearest neighboring hoppings between the same orbitals mediated by the As ions B and A, respectively. t_4 is the next nearest neighboring hopping between the different orbitals.

the next nearest neighboring hoppings between the same orbitals mediated by As ions B and A, respectively, and t_4 is the hopping between the different orbitals on the next nearest neighboring Fe sites (see Fig. 1). It is expected that t_4 is small and has the same value in both translation symmetry directions. Therefore, the model Hamiltonian we propose can be written as

$$H_0 = -\sum_{\alpha ij\sigma}\{\mu(c^\dagger_{A\alpha,ij\sigma}c_{A\alpha,ij\sigma} + c^\dagger_{B\alpha,ij\sigma}c_{B\alpha,ij\sigma}) + [t_1 c^\dagger_{A\alpha,ij\sigma}(c_{B\alpha,ij\sigma} + c_{B\alpha,i+1j\sigma} + c_{B\alpha,ij+1\sigma} + c_{B\alpha,i+1j+1\sigma}) + t_2(c^\dagger_{A\alpha,ij\sigma}c_{A\alpha,i+1j\sigma} + c^\dagger_{B\alpha,ij\sigma}c_{B\alpha,ij+1\sigma}) + t_3(c^\dagger_{A\alpha,ij\sigma}c_{A\alpha,ij+1\sigma} + c^\dagger_{B\alpha,ij\sigma}c_{B\alpha,i+1j\sigma}) + t_4(c^\dagger_{A\alpha,ij\sigma}c_{A\alpha+1,i+1j\sigma} + c^\dagger_{A\alpha,ij\sigma}c_{A\alpha+1,ij+1\sigma} + c^\dagger_{B\alpha,ij\sigma}c_{B\alpha+1,i+1j\sigma} + c^\dagger_{B\alpha,ij\sigma}c_{B\alpha+1,ij+1\sigma}) + \text{H.c.}]\}, \quad (1)$$

where $c^\dagger_{A(B)\alpha,ij\sigma}$ ($c_{A(B)\alpha,ij\sigma}$) creates (destroys) an α electron with spin σ in the unit cell $\{i, j\}$ of the sublattice A (B), and $\alpha = 0$ and 1 represent the degenerate orbitals d_{xz} and d_{yz}, respectively. Obviously, H_0 possesses the same symmetry with FeAs-based superconductors, which is key to understanding the electronic properties of this new family of high temperature superconductors.

To obtain the energy band structure of FeAs-based superconductors, we diagonalize the tight-binding model (1) in momentum space. Introducing $c_{A(B)\alpha,ij\sigma} = \frac{1}{\sqrt{N}}\sum_{\mathbf{k}} c_{A(B)\alpha,\mathbf{k}\sigma}e^{i(k_x x_i + k_y y_j)}$ with N the number of unit cells and taking the canonical transformation

$$\begin{pmatrix} c_{A0,\mathbf{k}\sigma} \\ c_{A1,\mathbf{k}\sigma} \\ c_{B0,\mathbf{k}\sigma} \\ c_{B1,\mathbf{k}\sigma} \end{pmatrix} = \begin{pmatrix} \frac{a_{0,\mathbf{k}}}{\Gamma_{0,\mathbf{k}}} & \frac{a_{0,\mathbf{k}}}{\Gamma_{0,\mathbf{k}}} & \frac{a_{1,\mathbf{k}}}{\Gamma_{1,\mathbf{k}}} & \frac{a_{1,\mathbf{k}}}{\Gamma_{1,\mathbf{k}}} \\ \frac{a_{0,\mathbf{k}}}{\Gamma_{0,\mathbf{k}}} & -\frac{a_{0,\mathbf{k}}}{\Gamma_{0,\mathbf{k}}} & \frac{a_{1,\mathbf{k}}}{\Gamma_{1,\mathbf{k}}} & -\frac{a_{1,\mathbf{k}}}{\Gamma_{1,\mathbf{k}}} \\ \frac{\epsilon^*_{T,\mathbf{k}}}{\Gamma_{0,\mathbf{k}}} & \frac{\epsilon^*_{T,\mathbf{k}}}{\Gamma_{0,\mathbf{k}}} & \frac{\epsilon^*_{T,\mathbf{k}}}{\Gamma_{1,\mathbf{k}}} & \frac{\epsilon^*_{T,\mathbf{k}}}{\Gamma_{1,\mathbf{k}}} \\ \frac{\epsilon^*_{T,\mathbf{k}}}{\Gamma_{0,\mathbf{k}}} & -\frac{\epsilon^*_{T,\mathbf{k}}}{\Gamma_{0,\mathbf{k}}} & \frac{\epsilon^*_{T,\mathbf{k}}}{\Gamma_{1,\mathbf{k}}} & -\frac{\epsilon^*_{T,\mathbf{k}}}{\Gamma_{1,\mathbf{k}}} \end{pmatrix} \begin{pmatrix} \psi_{00,\mathbf{k}\sigma} \\ \psi_{01,\mathbf{k}\sigma} \\ \psi_{10,\mathbf{k}\sigma} \\ \psi_{11,\mathbf{k}\sigma} \end{pmatrix}, \quad (2)$$

where $\psi_{uv,\mathbf{k}\sigma}$ are new fermion operators, $u(v) = 0, 1$, $\Gamma_{u,\mathbf{k}} = \sqrt{2(a^2_{u,\mathbf{k}} + \epsilon_{T,\mathbf{k}}\epsilon^*_{T,\mathbf{k}})}$, $a_{u,\mathbf{k}} = \frac{1}{2}(\epsilon_{A,\mathbf{k}} - \epsilon_{B,\mathbf{k}}) + (-1)^u\sqrt{\frac{1}{4}(\epsilon_{A,\mathbf{k}} - \epsilon_{B,\mathbf{k}})^2 + \epsilon_{T,\mathbf{k}}\epsilon^*_{T,\mathbf{k}}}$, $\epsilon_{A,\mathbf{k}} = -2(t_2\cos k_x + t_3\cos k_y)$, $\epsilon_{B,\mathbf{k}} = -2(t_2\cos k_y + t_3\cos k_x)$, $\epsilon_{xy,\mathbf{k}} = -2t_4(\cos k_x + \cos k_y)$, and $\epsilon_{T,\mathbf{k}} = -t_1[1 + e^{ik_x} + e^{ik_y} + e^{i(k_x+k_y)}]$, then we have

$$H_0 = \sum_{uv\mathbf{k}\sigma}(E_{uv,\mathbf{k}} - \mu)\psi^\dagger_{uv,\mathbf{k}\sigma}\psi_{uv,\mathbf{k}\sigma},$$
$$E_{uv,\mathbf{k}} = \frac{1}{2}(\epsilon_{A,\mathbf{k}} + \epsilon_{B,\mathbf{k}}) + (-1)^v\epsilon_{xy,\mathbf{k}} + (-1)^u\sqrt{\frac{1}{4}(\epsilon_{A,\mathbf{k}} - \epsilon_{B,\mathbf{k}})^2 + \epsilon_{T,\mathbf{k}}\epsilon^*_{T,\mathbf{k}}}. \quad (3)$$

Here, we have set the lattice constant $a = 1$.

Equation (3) describes analytically four energy bands with the indexes $\langle u, v\rangle$. In Fig. 2, we plot these bands along the path $(0, 0) \to (\pi, 0) \to (\pi, \pi) \to (0, 0)$. In our calculations, we have used $t_1 = 0.5$, $t_2 = 0.2$, $t_3 = -1.0$, $t_4 = 0.02$, and $\mu = -0.622$ (half filling) (eV). Obviously, there exist two hole Fermi surfaces around (0,0), i.e., α and β bands, and two electron Fermi surfaces around (π, π), i.e., γ and δ bands. We note that the hole and electron pockets are associated with $u = 1$ and 0 while $v = 0$ and 1 represent the inner and outer Fermi surfaces of the hole and electron pockets, respectively. The parameters t_1, t_2, and t_3 determine the sizes of the hole and electron pockets, and t_4 controls the intervals between the inner and outer Fermi surfaces. We also note that $\mu < -0.622$ and $\mu > -0.622$ correspond to hole and electron dopings, respectively. With increasing hole (electron) doping, the hole (electron) Fermi surfaces, i.e., α and β bands (γ and δ bands), become larger while the electron (hole) Fermi surfaces, i.e., γ- and δ bands (α- and β- bands) become smaller. When $\mu > -0.48$ (i.e., $\sim$15.9% electron doping), α band does not exist. If $\mu > -0.32$ (i.e., $\sim$26.5% electron doping), β band also disappears. Therefore, the energy band structure described by Eq. (3) agrees qualitatively with the observations of ARPES experiments in the whole range of electron and hole dopings [7–15].

In order to investigate superconductivity in iron arsenides, we now introduce the pairing Hamiltonian

$$H_{\text{SC}} = \sum_{uv\mathbf{k}}(\Delta_{uv,\mathbf{k}}\psi^\dagger_{uv,\mathbf{k}\uparrow}\psi^\dagger_{uv,-\mathbf{k}\downarrow} + \text{H.c.}), \quad (4)$$

where $\Delta_{uv,\mathbf{k}}$ are the superconducting gaps on the energy bands $\langle u, v\rangle$, depending on the momentum of the quasiparticles $\psi_{uv,\mathbf{k}\sigma}$. Here, we assume that the energy gaps on

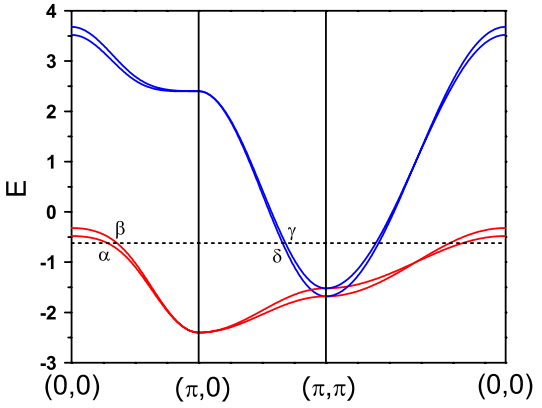

FIG. 2 (color online). The band structure of the four-band model with $t_1 = 0.5$, $t_2 = 0.2$, $t_3 = -1.0$, $t_4 = 0.02$, and $\mu = -0.622$ (eV), plotted along the path $(0, 0) \to (\pi, 0) \to (\pi, \pi) \to (0, 0)$.

all the Fermi surfaces can be described by a single function of the momentum, i.e., $\Delta_{10,\mathbf{k}} = \Delta_{11,\mathbf{k}} = \Delta_{00,\mathbf{k}} = \Delta_{01,\mathbf{k}}$. In Ref. [12], Nakayama *et al.* measured the energy gaps on different Fermi surfaces in optimally hole-doped $Ba_{0.6}K_{0.4}Fe_2As_2$ ($T_c \sim 37$ K) by employing ARPES experiments. The order parameter can be fitted as $\Delta_{uv,\mathbf{k}} = \frac{1}{2}\Delta_0(\cos k_x + \cos k_y)$ with $\Delta_0 = 13.5$ meV or $|\Delta_{uv,\mathbf{k}}|$ in the present coordinate system (i.e., two Fe ions per unit cell). Such an energy gap can be induced by antiferromagnetic spin fluctuations on the same Fe sublattices [17,20]. However, in the STM experiments on optimally electron-doped $BaFe_{1.8}Co_{0.2}As_2$ ($T_c \sim 22.5$ K) [29–31], only two coherence peaks were observed at a small gap, i.e., $\sim \pm 5.8$ meV. In the following we shall calculate the differential conductance for the extended s-wave pairing symmetry in the optimal electron doping, so that we can compare our theory with the STM experiments.

After diagonalizing the mean field BCS Hamiltonian $H = H_0 + H_{\mathrm{SC}}$ by the Bogoliubov transformation, we obtain the local density of states (LDOS) on the sublattice A or B

$$\rho_{A,B}(\omega) = -\frac{4}{N\pi}\sum_{uv\mathbf{k}\nu}\frac{\mathcal{A}^{A,B}_{u,\mathbf{k}}\xi^2_{uv,\mathbf{k}\nu}}{i\omega_n - (-1)^\nu\Omega_{uv,\mathbf{k}}}\Bigg|_{i\omega_n\to\omega+i0^+}, \quad (5)$$

where $\nu = \pm 1$, $\mathcal{A}^{A}_{u,\mathbf{k}} = a^2_{u,\mathbf{k}}/\Gamma^2_{u,\mathbf{k}}$, $\mathcal{A}^{B}_{u,\mathbf{k}} = \epsilon_{T,\mathbf{k}}\epsilon^*_{T,\mathbf{k}}/\Gamma^2_{u,\mathbf{k}}$, $\Omega_{uv,\mathbf{k}} = \sqrt{(E_{uv,\mathbf{k}} - \mu)^2 + \Delta^2_{uv,\mathbf{k}}}$, and $\xi^2_{uv,\mathbf{k}\nu} = \frac{1}{2}[1 + (-1)^\nu\frac{E_{uv,\mathbf{k}} - \mu}{\Omega_{uv,\mathbf{k}}}]$. Obviously, the quasiparticles on the hole and electron pockets have different weights $\mathcal{A}^{A,B}_{u,\mathbf{k}}$ to contribute to the LDOS.

Usually STM experiments are performed at low temperatures. In order to compare accurately with STM experiments, we must take the effect of temperature into account. The differential conductance measured by STM experiments is

$$\frac{dI}{dV} \propto -\int_{-\infty}^{\infty} f'(\omega - eV)\rho_{A,B}(\omega)d\omega, \quad (6)$$

where f' is the derivative of the Fermi function and V is the bias voltage applied between STM tip and sample.

According to formulas (5) and (6), we can calculate differential conductance with different pairing symmetries and dopings at low temperatures. In Fig. 3(a), we present differential conductance for extended s-wave symmetry with optimal electron doping under temperature 4.2 K. The coherence peaks locate at $\pm\Delta_0$. We have observed that the main contribution to dI/dV comes from the hole Fermi surfaces, i.e., α and β bands. The main difference between theoretical results and the STM data could be due to the fact that either the β or δ band of the STM sample is much closer to the nodal line as depicted in Fig. 3(b).

In order to detect the sign-reversal pairing in the FeAs-based superconductors, now we calculate the LDOS near an impurity located at the origin of the sublattice A described by $H_{\mathrm{imp}} = V_s\sum_{\alpha\sigma}c^+_{A\alpha,00\sigma}c_{A\alpha,00\sigma} + V_m\sum_\alpha(c^+_{A\alpha,00\uparrow}c_{A\alpha,00\uparrow} - c^+_{A\alpha,00\downarrow}c_{A\alpha,00\downarrow})$. Here, V_s and V_m represent the nonmagnetic part and magnetic part of the impurity potential, respectively. The total Hamiltonian $H = H_0 + H_{\mathrm{SC}} + H_{\mathrm{imp}}$ can be solved by the T-matrix approach [32]. The analytical expression for the LDOS on the sublattices A and B near the impurity has been derived and will be presented elsewhere. We note that the interband scattering is only allowed for those bands with the same index v.

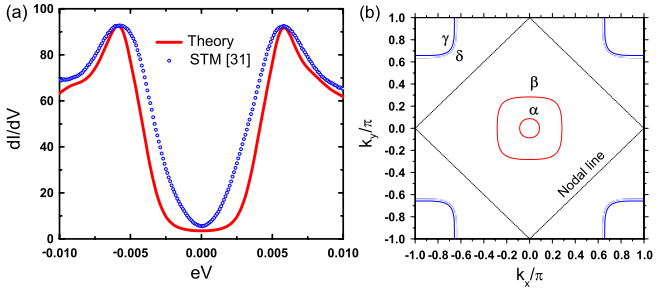

FIG. 3 (color online). (a) The differential conductance as a function of the bias voltage eV for the pairing symmetry $\Delta_{uv,\mathbf{k}} = \frac{1}{2}\Delta_0(\cos k_x + \cos k_y)$ with $\Delta_0 = 5.8$ meV and $|\Delta_{uv,\mathbf{k}}|$ at optimal electron doping (~15%) under temperature 4.2 K. (b) The corresponding Fermi surfaces.

In Fig. 4, we plot the LDOS curves for $\Delta_{uv,\mathbf{k}}$ and $|\Delta_{uv,\mathbf{k}}|$ on and near the impurity site with a moderate strength of nonmagnetic potential, i.e., $V_s = 0.25$ eV, plus a small magnetic potential, i.e., $V_m = 0.08$ eV. Obviously, for a pure scattering potential ($V_m = 0$), the LDOS for $\Delta_{uv,\mathbf{k}}$ has two impurity resonance peaks at $\pm\omega_0 = \pm 2.8$ meV on the impurity site and has a sharp resonance peak at ω_0 near the impurity site. However, the LDOS for $|\Delta_{uv,\mathbf{k}}|$ has no such in-gap impurity states due to no pair-breaking effect. Therefore, these impurity resonances can be used to detect the sign-reversal pairing in the FeAs-based superconductors. The origin of these impurity resonances comes from the Andreev's bound states due to interband quasiparticle scattering with the phase opposite order parameters, similar to that of the zero bias resonance peak on a Zn impurity in cuprate superconductors. An additional small magnetic potential can strongly suppress the impurity peak at $-\omega_0$ and enhance the impurity peak at ω_0 on the impurity site. Meanwhile, all the resonance peaks on different sites slowly move forward to zero energy. We note that for the mixing potential, the LDOS for $|\Delta_{uv,\mathbf{k}}|$ is similar to that induced by a magnetic impurity in s-wave superconductors.

Figure 5 shows the LDOS for $\Delta_{uv,\mathbf{k}}$ and $|\Delta_{uv,\mathbf{k}}|$ near the impurity site with a unitary potential. The LDOS for $\Delta_{uv,\mathbf{k}}$ also has two impurity resonance peaks at $\pm\omega_0$. However, the resonance peak at $-\omega_0$ is much stronger than that at ω_0. For $|\Delta_{uv,\mathbf{k}}|$, the LDOS also has no in-gap impurity resonance peaks.

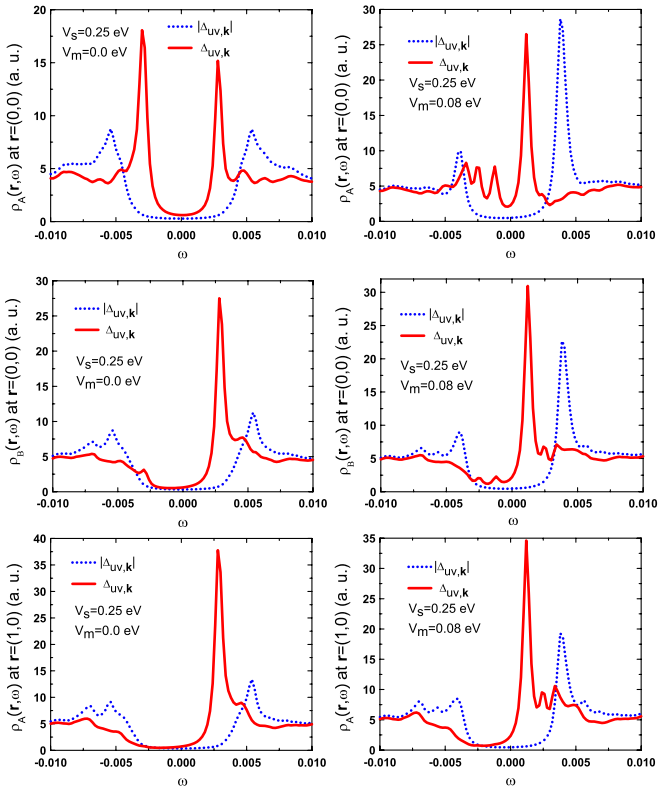

FIG. 4 (color online). The LDOS near an impurity, which includes a dominant nonmagnetic potential V_s and a small magnetic part V_m, for the pairing symmetry $\Delta_{uv,\mathbf{k}} = \frac{1}{2}\Delta_0(\cos k_x + \cos k_y)$ with $\Delta_0 = 5.8$ meV and $|\Delta_{uv,\mathbf{k}}|$ at optimal electron doping ($\sim$15%).

We also investigate the other cases of the impurity potential. For the attractive scattering potential, i.e., $V_s < 0$, the stronger resonance peak inside gap in the LDOS near the impurity site always appears at negative energy. With increasing $|V_s|$, the resonance peaks become higher. When $V_s \to -\infty$, the LDOS is identical with that for $V_s \to +\infty$, shown in Fig. 5. We note that an extra small magnetic potential does not change the features of the LDOS. For a dominantly magnetic potential, which always breaks Cooper pairs, the LDOS near the impurity site for $\Delta_{uv,\mathbf{k}}$ has similar peak structures with that for $|\Delta_{uv,\mathbf{k}}|$, although the values of V_m or the locations of in-gap resonance peaks are different. Therefore, magnetic impurity seems not to be a good tool for detecting sign-reversal pairing in FeAs-based superconductors.

In summary, we have built a two-orbital four-band tight-binding model by starting directly from two Fe ions per unit cell for the first time. The energy band structure describes correctly the characteristics of Fermi surfaces in FeAs-based superconductors. It is shown that in-gap impurity resonances induced by nonmagnetic scattering potential can be regarded as a signature of sign-reversal pairing in FeAs-based superconductors, which could be detected by STM experiments.

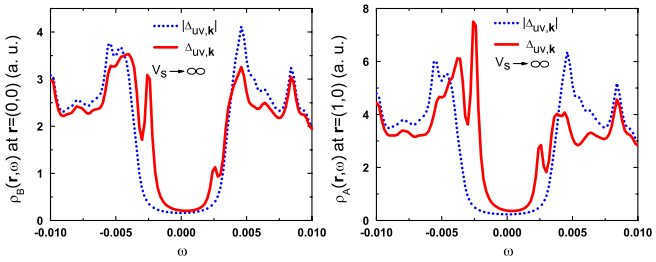

FIG. 5 (color online). The LDOS near a unitary impurity for the pairing symmetry $\Delta_{uv,\mathbf{k}} = \frac{1}{2}\Delta_0(\cos k_x + \cos k_y)$ with $\Delta_0 = 5.8$ meV and $|\Delta_{uv,\mathbf{k}}|$ at optimal electron doping ($\sim$15%).

The author would like to thank C. S. Ting, S. H. Pan, Ang Li, and Tao Zhou for useful discussions, and especially S. H. Pan and Ang Li for providing me their STM data. This work was supported by the Texas Center for Superconductivity at the University of Houston and by the Robert A. Welch Foundation under Grant No. E-1146.

[1] Y. Kamihara *et al.*, J. Am. Chem. Soc. **130**, 3296 (2008).
[2] Z. A. Ren *et al.*, Chin. Phys. Lett. **25**, 2215 (2008).
[3] X. H. Chen *et al.*, Nature (London) **453**, 761 (2008).
[4] C. de la Cruz *et al.*, Nature (London) **453**, 899 (2008).
[5] G. F. Chen *et al.*, Phys. Rev. Lett. **100**, 247002 (2008).
[6] H.-H Wen *et al.*, Europhys. Lett. **82**, 17009 (2008).
[7] H. Ding *et al.*, Europhys. Lett. **83**, 47001 (2008).
[8] D. H. Lu *et al.*, Nature (London) **455**, 81 (2008).
[9] C. Liu *et al.*, Phys. Rev. Lett. **101**, 177005 (2008).
[10] T. Kondo *et al.*, Phys. Rev. Lett. **101**, 147003 (2008).
[11] D. V. Evtushinsky *et al.*, Phys. Rev. B **79**, 054517 (2009).
[12] K. Nakayama *et al.*, Europhys. Lett. **85**, 67002 (2009).
[13] V. Zabolotnyy *et al.*, Nature (London) **457**, 569 (2009).
[14] K. Terashima *et al.*, Proc. Natl. Acad. Sci. U.S.A. **106**, 7330 (2009).
[15] Y. Sekiba *et al.*, New J. Phys. **11**, 025020 (2009).
[16] D. J. Singh and M. H. Du, Phys. Rev. Lett. **100**, 237003 (2008).
[17] I. I. Mazin *et al.*, Phys. Rev. Lett. **101**, 057003 (2008).
[18] K. Haule, J. H. Shim, and G. Kotliar, Phys. Rev. Lett. **100**, 226402 (2008).
[19] G. Xu *et al.*, Europhys. Lett. **82**, 67002 (2008).
[20] K. Kuroki *et al.*, Phys. Rev. Lett. **101**, 087004 (2008).
[21] X. Dai *et al.*, Phys. Rev. Lett. **101**, 057008 (2008).
[22] S. Raghu *et al.*, Phys. Rev. B **77**, 220503(R) (2008).
[23] P. A. Lee and X.-G. Wen, Phys. Rev. B **78**, 144517 (2008).
[24] Zi-Jian Yao *et al.*, New J. Phys. **11**, 025009 (2009).
[25] Y. Ran *et al.*, Phys. Rev. B **79**, 014505 (2009).
[26] T. Y. Chen *et al.*, Nature (London) **453**, 1224 (2008).
[27] L. Shan *et al.*, Europhys. Lett. **83**, 57004 (2008).
[28] O. Millo *et al.*, Phys. Rev. B **78**, 092505 (2008).
[29] Y. Yin *et al.*, Phys. Rev. Lett. **102**, 097002 (2009).
[30] F. Massee *et al.*, Phys. Rev. B **79**, 220517(R) (2009).
[31] Ang Li *et al.* (to be published).
[32] A. V. Balatsky, I. Vekhter, and J.-X. Zhu, Rev. Mod. Phys. **78**, 373 (2006).